Gel-Mediated Electrospray Assembly of Silica Supraparticles for Sustained Drug Delivery

Yutian Ma,[†] Mattias Björnmalm,[†,¶,‡] Andrew K. Wise,[¶,#] Christina Cortez-Jugo,[†] Eve Revalor,[§,¤] Yi Ju,[†] Orlagh M. Feeney,[⊥] Rachael Richardson,[¶] Eric Hanssen,[Δ] Robert K. Shepherd,[¶,#] Christopher J. H. Porter,[⊥] and Frank Caruso*,[†]

[†]ARC Centre of Excellence in Convergent Bio-Nano Science and Technology, and the Department of Chemical Engineering, The University of Melbourne, Parkville, Victoria 3010, Australia.

[¶]Bionics Institute, East Melbourne, Victoria 3002, Australia.

[‡]Department of Materials, Department of Bioengineering, and the Institute of Biomedical Engineering, Imperial College London, London SW7 2AZ, UK.

[#]Department of Medical Bionics and Department of Otolaryngology, The University of Melbourne, Parkville, Victoria 3010, Australia.

[§]Melbourne Medical School, Faculty of Medicine, Dentistry & Health Sciences, The University of Melbourne, Parkville, Victoria 3010, Australia

[¤]Department of Biomedical Engineering, The University of Melbourne, Parkville, Victoria 3010, Australia.

[⊥]ARC Centre of Excellence in Convergent Bio-Nano Science and Technology, and Drug Delivery Disposition and Dynamics, Monash Institute of Pharmaceutical Sciences, Monash University, Parkville, Victoria 3052, Australia.

[Δ]Melbourne Advanced Microscopy Facility and Department of Biochemistry and Molecular Biology, Bio21 Molecular Science and Biotechnology Institute, The University of Melbourne, Parkville, Victoria 3010, Australia.

*E-mail: fcaruso@unimelb.edu.au

KEYWORDS: alginate, electrospray, silica supraparticles, porous silica, drug delivery

ABSTRACT

Supraparticles (SPs) composed of smaller colloidal microparticles provide a platform for the long-term, controlled release of therapeutics in biomedical applications. However, current synthesis methods used to achieve high drug loading and that involve biocompatible materials are often tedious, thereby limiting the translation of SPs to diverse applications. Herein, we present a simple, effective, and automatable alginate-mediated electrospray technique for the assembly of robust spherical silica SPs (Si-SPs) for long-term (>4 months) drug delivery. The Si-SPs are composed of either porous or nonporous primary Si microparticles within a decomposable alginate matrix. The size and shape of Si-SPs can be tailored by controlling the concentrations of alginate and silica microparticles used and key electrospraying parameters such as flow rate, voltage, and collector distance. Furthermore, the performance (including drug loading kinetics, loading capacity, loading efficiency, and drug release) of the Si-SPs can be tuned by changing the porosity of the primary particles and through the retention or removal (via calcination) of the alginate matrix. The structure and morphology of the Si-SPs were characterized by electron microscopy, dynamic light scattering, N_2 adsorption–desorption analysis, and X-ray photoelectron spectroscopy. The cytotoxicity and degradability of the Si-SPs were also examined. Drug loading kinetics and loading capacity for six different types of Si-SPs, using a model protein drug (fluorescently labeled lysozyme), demonstrate that Si-SPs prepared from primary silica particles with large pores can load significant amounts of lysozyme (~10 µg per SP) and exhibit sustained, long-term release of more than 150 days. Our experiments show that Si-SPs can be produced through a gel-mediated electrospray technique that is robust and automatable (important for clinical translation and commercialization), and that they present a promising platform for long-term drug delivery.

INTRODUCTION

Colloidal particles can exhibit a range of properties (e.g., electronic, magnetic, optical, and catalytic), making them suitable for application in diverse disciplines such as chemistry, physics, engineering, and biomedicine.[1–4] Supraparticles (SPs) are assemblies (clusters) of primary colloidal particles, and their size typically ranges from micrometers to millimeters.[5] As the size and structure of a material can significantly influence its mechanical and physicochemical properties, SPs can thus exhibit substantially different properties from their individual primary (colloidal) particle counterparts.[6,7] SPs have been applied in various fields including photonics (as light-diffracting "opal balls"[8], and colored films[7,9]), biosensing,[10] catalysis,[11] and water remediation.[12] In the field of biomedicine, SPs can serve as carriers for loading and delivering drugs. Examples include porous latex SPs for the continuous release of solutes (e.g., dye)[13] and functionalized magnetic SPs for targeted drug delivery applications.[14] Nonetheless, there exists an ongoing need to develop SPs with a high drug loading capacity and with release properties appropriate for the intended application, within a biocompatible matrix that is safe to use in vivo. Additionally, many of the SP systems developed to date are typically assembled through manual, time-consuming preparation steps, and robust, automatable assembly procedures are therefore of interest to facilitate translation into diverse applications.

Recently, we reported a biocompatible inner ear drug delivery system using mesoporous Si-SPs loaded with brain-derived neurotrophic factor (BDNF), a naturally occurring protein that is expressed by certain types of cells within the inner ear and may have therapeutic benefits after hearing loss.[15–17] These BDNF-loaded SPs address some of the concerns associated with safety and efficiency of drug delivery to the inner ear and have been shown to improve the survival of auditory neurons after hearing loss in vivo.[17–21] The BDNF-loaded SPs (composed of millions of

primary silica particles) have been synthesized by evaporation-induced self-assembly (EISA)[2,5,21] or a mold-templating approach.[22] In the EISA method, aqueous droplets containing primary silica particles are evaporated on a hydrophobic surface (e.g., paraffin film) and as the droplet dries out, the suspended primary silica particles aggregate until they form a SP (when all liquid has evaporated).[21] In the mold-templating method, primary silica particles are mixed with gelatin (which acts as a biodegradable adhesive), and this mixture is then added to microfabricated wells in the mold followed by drying in vacuum.[22] The mixture in each well dries out and results in a semi-spherical SP, which can be recovered by inverting the mold.[22] The challenges of these two methods include long processing times and extensive manual handling by a skilled user to reproducibly generate SPs, making SPs difficult to translate into larger scale production processes needed for widespread application. Given these limitations, a simple, automatable method that is able to rapidly produce Si-SPs in large scale, with concurrent high drug loading capacity and controlled release behavior, would be attractive for advancing SP technologies towards clinical translation.

To address these issues, herein, we develop a robust and automatable alginate gel-mediated electrospray method for SP assembly. Alginate is a natural polysaccharide extracted from brown seaweed that can be used for diverse applications owing to its high biocompatibility.[23,24] Primary silica particles were encapsulated in alginate to form alginate/silica supraparticles (Si-SPs^{alg}) crosslinked with ionic agents (e.g., Ca^{2+}), as illustrated in Scheme 1 and Figure S1.[23–26] While a variety of electrospraying techniques have been applied to produce a wide range of nano- and microparticles, including alginate-based beads,[27,28] the electrospray technique presented here produces large alginate/silica SPs (>100 μm) with improved preparation efficiency: thousands of SPs can be assembled in 30 min, which would take many weeks to manually prepare through

EISA.[21] The electrospray technique also results in robust, spherical SPs with uniform size and requires minimal manual intervention: important properties for quality control, translational into clinical applications, and commercialization. When incubated with a human brain glioblastoma cell line (U87MG), negligible cytotoxicity was observed with the SPs. Protein encapsulation studies using a fluorescently labeled model protein (fluorescein isothiocyanate (FITC)-lysozyme) and six different types of SPs were conducted to assess the drug loading capacity and the drug release kinetics of the SPs. The SPs were prepared from three different types of primary silica particles that were nonporous, or contained small or large pores, and alginate was either retained or removed (via calcination) in the SP systems (see Table S1 for details). The in vitro drug release behavior of both FITC-lysozyme-loaded SPs and BDNF-loaded SPs showed improved release properties when compared with that of our previous SP systems.[21] Particularly, our results show that Si-SPs prepared using primary silica particles with large pores (^{L}Si-SPs) and in which the alginate matrix was removed (via calcination) may be a promising platform for long-term (>4 months) controlled drug delivery and would be suitable for therapeutic approaches requiring sustained delivery, for instance, neurotrophin delivery to the inner ear to treat hearing loss.

EXPERIMENTAL METHODS

Materials. Tetraethyl orthosilicate (TEOS), poly(acrylic acid) (PAA, M_w ~250 kDa, 35 wt% solution in water), ammonium hydroxide solution (28–30%), cetyltrimethylammonium bromide (CTAB), Pluronic F127 (PF127), FITC, lysozyme protein from chicken egg white, alginic acid sodium salt from brown algae (alginate), calcium chloride (CaCl$_2$), mesoporous silica particles (diameter ~0.5 μm, pore size ~2 nm), phosphate-buffered saline (PBS, pH 7.4), sodium tetraborate (Na$_2$B$_4$O$_7$), sodium phosphate monobasic monohydrate, and 4-(2-hydroxyethyl)piperazine-1-ethanesulfonic acid (HEPES) were purchased from Sigma-Aldrich (USA). Sodium acetate

anhydrous, sodium hydrogen carbonate, and hydrochloric acid were purchased from Chem-Supply (Australia). Boric acid (H_3BO_3) was obtained from M&B (Australia). Sodium hydroxide was obtained from Univar (Australia). Nonporous silica particles (diameter 0.5 ± 0.013 μm, 5 wt% aqueous dispersion) were purchased from microParticles GmbH (Germany). Alamar Blue cell viability reagent was obtained from Life Technologies (USA). The U87MG human brain glioblastoma cell line was purchased from American Type Culture Collection (ATCC, USA), and the BDNF human protein was purchased from GenWay Biotech. Inc. (USA). Human BDNF ELISA kits were obtained from Abcam (Australia). Ultrapure water (Milli-Q) with a resistivity of greater than 18 MΩ cm was used in all experiments and obtained from a three-stage Millipore Milli-Q Plus 185 purification system. All chemicals were used without further purification.
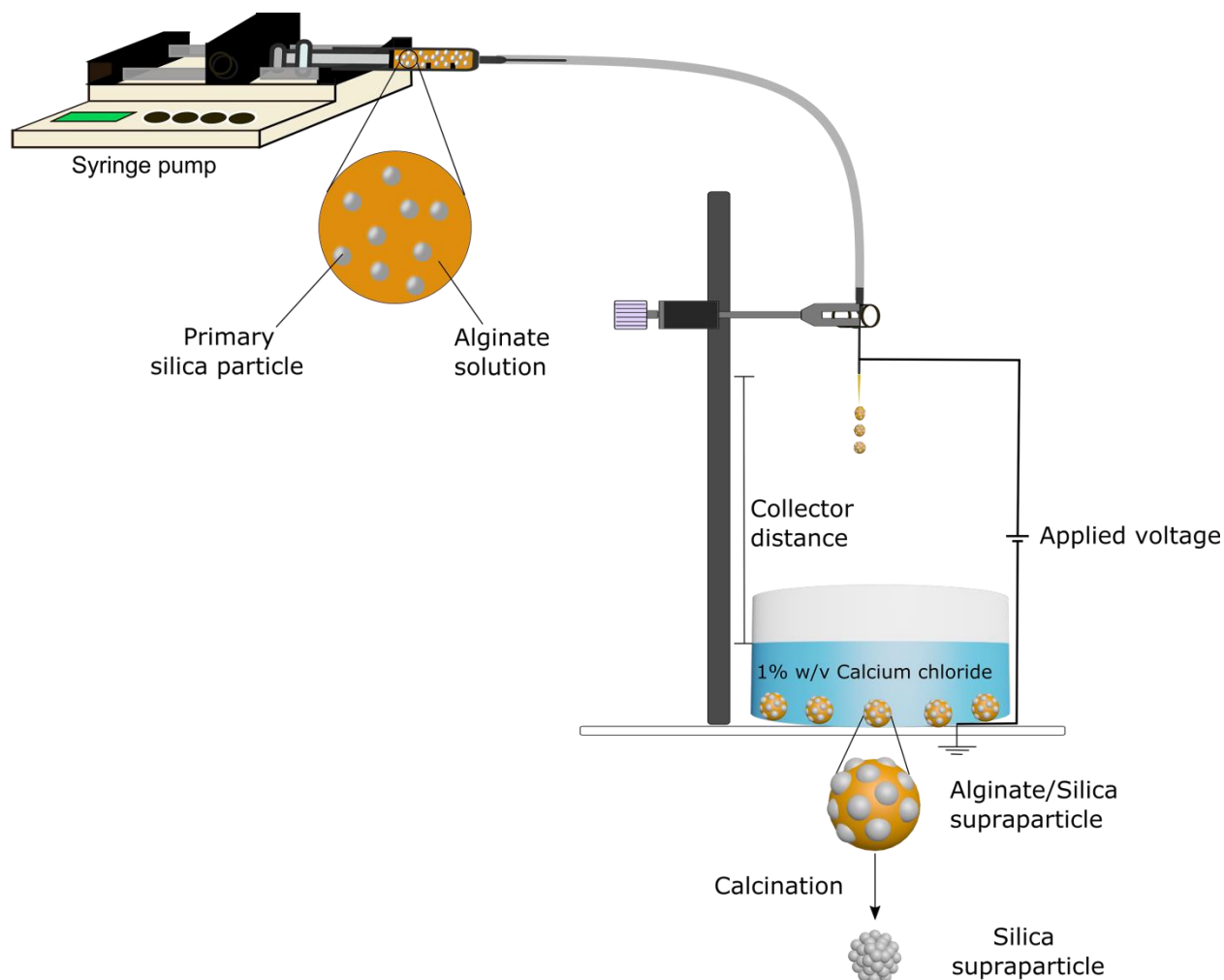
Synthesis of Primary Silica Particles with Large Pores. Primary silica particles of ~1 μm in diameter with large pores (see Table S1) were prepared using a modified version of a previously published protocol.[29] Briefly, 1.1 g of CTAB was suspended in 50 mL of Milli-Q water and then mixed with 4.3 g of PAA under vigorous stirring at room temperature (~22 °C). After 20 min, a clear solution was obtained, to which 3.5 mL of ammonium hydroxide solution (28–30%) was added with vigorous stirring for 20 min, yielding a milky suspension. Subsequently, 4.46 mL of TEOS was added to the above suspension with vigorous stirring for 15 min. Then, the mixture was placed into a Teflon-sealed autoclave at 90 °C. After 48 h, the silica particles were removed from the Teflon-sealed autoclave and washed with Milli-Q water and ethanol twice, and then dried at 80°C. Finally, the silica particles were placed in a chamber furnace (Jetlow, Australia) and calcined at 823 K for 30 h to remove any organic materials.

Synthesis of Silica Supraparticles. The Si-SPs were synthesized using the electrospray setup depicted in Scheme 1 and Figure S2. Three types of primary silica particles were used: (1)

nonporous silica particles (microParticles GmbH); (2) silica particles with small pores (2 nm; Sigma-Aldrich); and (3) silica particles with large pores (2–3, 15–64, >100 nm; synthesized in-house) (See Table S1 for additional details).

As an example, for the synthesis of Si-SPs with a diameter of approximately 550 µm, 80 mg of primary silica particles with large pores was dispersed in 2 mL of alginate aqueous solution (30 mg mL^{-1} in Milli-Q water). After mixing, the suspension was ultra-sonicated using an ultrasonic processor with a microtip probe (Qsonica, CT, USA) at an output amplitude of 30% for 40 s and sonicated further in an ultrasonic cleaner (Branson, USA) for 1 h to ensure that the primary silica particles were distributed evenly within the alginate solution. Subsequently, the solution was drawn into a syringe and positioned in a syringe pump programmed to deliver a constant flow rate of 8 mL h^{-1}. A 17-gauge nozzle and 13 kV applied voltage were used in the electrospray setup to drip the alginate/primary silica particle solution into a 1% w/v of CaCl$_2$ dissolved in Milli-Q water, as the gelling bath. The calcium chloride crosslinked with the alginate to form alginate beads. After 5 min, the alginate/silica supraparticles (Si-SPs^{alg}) were collected directly from the calcium chloride bath using a strainer and washed in Milli-Q water (Figure S3a). The SPs were washed 4–5 times with fresh Milli-Q water with the supernatant removed between washes and then stored in Milli-Q water. The alginate was then removed by calcination at 923 K for 30 h to produce the Si-SPs.

The size of the Si-SPs was varied by adjusting several parameters such as flow rate, applied voltage, distance between the crosslinker solution and nozzle, and the concentration of alginate or primary silica particles with large pores. The influence of varying these parameters is discussed below and the results are summarized in Table 1.

Scheme 1. Schematic illustration of the electrospray synthesis of SPs. A solution of alginate containing primary silica particles is pumped through a nozzle, and as voltage is applied, droplets of alginate/silica form and are collected in a calcium chloride bath, which crosslinks the alginate to form SPs. Upon subsequent calcination (at 923 K for 30 h) to remove alginate, Si-SPs are obtained. (See Figure S2 for photographs of the setup.)

Characterization. Transmission electron microscopy (TEM) images of the primary silica particles were taken with a FEI Tecnai TF20 instrument (FEI, USA) with an operation voltage of 200 kV. The TEM samples were prepared by dropping 2 µL of diluted samples (in Milli Q water)

on Formvar carbon-coated copper grids. Scanning electron microscopy (SEM) images of the primary silica particles with large pores and [L]Si-SPs were taken using a Philips XL30 field-emission scanning electron microscope (Philips, Netherlands) at an operating voltage of 10 kV. SEM images of the [S]Si-SPs and [N]Si-SPs were taken using a TM4000 PLUS tabletop scanning electron microscope (HITACHI, Tokyo, Japan) at an operating voltage of 15 kV. SEM samples of the primary silica particles with large pores were prepared by dropping an aqueous suspension of the particles dispersed in Milli-Q water directly onto glass slides followed by air drying. SEM samples of the SPs were prepared by placing them directly onto silica wafers and then coating them (via sputtering) with a thin layer of gold. Fluorescence microscopy images were obtained using a confocal laser scanning microscope (Leica, Germany) equipped with an argon laser. The inner structures of [L]Si-SPs were examined with a FEI Tecnai F30 cryo-electron microscope (FEI, USA) at an operating voltage of 300 kV. Tomograms were reconstructed using IMOD (image processing software, University of Colorado).[30] The size distribution and circularity distribution of [L]Si-SPs were determined using ImageJ software (NIH, USA) by processing images obtained with an Olympus IX71 inverted microscope. The circularity of the [L]Si-SPs was calculated using Equation 1, with the area and perimeter values estimated using Image J. Histograms were obtained using a software described elsewhere.[31]

$$\text{Circularity} = \frac{4 \times \pi \times \text{Area}}{\text{Perimeter}^2} \tag{1}$$

Zeta potentials of Si-SPs were determined using a Malvern Zetasizer Nano ZS (Malvern Instrument, Worcestershire, UK). A mortar and pestle was used to grind Si-SPs into a powder, which was then dispersed in 10 mM sodium acetate buffer (pH 4), phosphate buffer (pH 6), HEPES buffer (pH 8), or sodium bicarbonate buffer (pH 10) for microelectrophoresis measurements to determine the zeta potential. Porosity analysis of the primary silica particles was performed using

a Micrometrics ASAP2010 analyzer (Micrometrics, USA). Elemental composition of [L]Si-SPs was determined by X-ray photoelectron spectroscopy (XPS) on a VG ESCALAB220i-XL spectrometer. The force required to fracture individual SPs was determined by a force–fracture test (Figure S4). In this method, SPs were placed under a force transducer connected to a force gauge (Mark-10, Long Island, New York, USA), and the distance between the transducer and the SPs was reduced using a motorized micromanipulator (Sutter Instrument, Novato, USA) until a force was detected on the force gauge, corresponding to the SPs being in contact with the transducer. The force was then continuously monitored as the distance was reduced. The force measured upon fracture of the SPs was determined as the maximal force that the SPs could withstand.

Cytotoxicity. U87MG human brain glioblastoma cells were grown in DMEM supplemented with 10% fetal bovine serum at 37 °C in a 5% CO_2 incubator. U87MG cells were seeded in a 24-well Transwell plate at 1×10^4 cells per well in 400 µL of medium and incubated overnight. The [L]Si-SPs were then sterilized with 100 µL of ethanol (80% v/v) at room temperature (~22 °C) for 4 h. The [L]Si-SPs were then washed with sterile Milli-Q water, sterile PBS, and then the cell culture medium three times. The medium in each well was removed, and 500 µL of fresh medium was introduced into each well. Subsequently, different numbers of the sterilized [L]Si-SPs were added into Transwell membrane inserts, which were then placed in the receiving wells that contained the cells. The cells did not directly contact [L]Si-SPs, as the Transwell insert provided a porous barrier (with a diameter of 3.0 µm) between cells and the relatively large [L]Si-SPs. After 48 h of incubation, the Transwell inserts with the [L]Si-SPs were removed, and 50 µL of Alamar Blue reagent was added to each well, according to the manufacturer's instructions. After 6 h of incubation, the fluorescence intensity of the solution was measured using an Infinite M200 microplate reader with an excitation

wavelength of 540 nm and an emission wavelength of 610 nm. Samples containing only medium and Alamar Blue were used as background controls. Ethanol was added to cells with inserts as a cytotoxic control. Cells that had not been exposed to ^{L}Si-SPs were used as the untreated controls. The cell viability curve was then established based on these controls and the number of ^{L}Si-SPs incubated per well.

FITC Labeling of Lysozyme. Lysozyme was labeled as described previously with slight modifications.[32] Briefly, 4 mg of FITC was added to 20 mL of 100 mM borate buffer pH 9.0. Lysozyme (224.3 mg) was then added with vigorous stirring. The samples were covered with aluminum foil and stirred at room temperature (~22°C) for 90 min. To remove unreacted dye, the sample was dialyzed using SnakeSkin dialysis tubing (3.5 k molecular weight cutoff, Thermo Scientific) against Milli-Q water over 4 days with frequent (twice daily) water exchanges. The dialyzed FITC-lysozyme was then lyophilized. Borate buffer was prepared by mixing $Na_2B_4O_7$ and H_3BO_3, with its pH adjusted to 9.0.

Drug Loading. For the drug loading studies, six different types of Si-SPs were examined and denoted as ^{N}Si-SPs^{alg}, ^{S}Si-SPs^{alg}, ^{L}Si-SPs^{alg}, and ^{N}Si-SPs, ^{S}Si-SPs, ^{L}Si-SPs, where superscripts N, S, and L infer that the SPs were prepared from nonporous primary silica particles, primary silica particles with small pores, or primarily silica particles with large pores, respectively, and superscript alg infers that alginate was not removed, whereas the absence of superscript alg infers that alginate was removed by employing a calcination step. All Si-SPs were synthesized under the optimized electrospray conditions presented in row 3 (Table 1).

The FITC-lysozyme loading kinetics was assessed by adding FITC-lysozyme solution (0.6 mg mL^{-1} in Milli-Q water) to the six different types of SPs prepared (with 5 Si-SPs in each sample). First, the Si-SPs were sterilized with 100 μL of ethanol (80% v/v) at room temperature (~22 °C)

for 4 h. The SPs were then washed with sterile Milli-Q water six times. Next, 100 μL of FITC-lysozyme solution was added to the different types of Si-SPs. At defined time intervals between 4 and 120 h, 90 μL of supernatant was withdrawn for analysis. The concentration of FITC-lysozyme in the supernatant was measured using an Infinite M200 microplate reader (Tecan, Australia Pty. Ltd.), using an excitation wavelength of 490 nm and an emission wavelength of 525 nm, and determined using a standard curve. The amount of FITC-lysozyme loaded into the different types of Si-SPs at each time point was calculated by subtracting the amount of FITC-lysozyme in the supernatant from the amount of FITC-lysozyme in the original stock solution (i.e., the pre-loaded solution minus the post-loaded solution), according to Equation 2:

$$q_t = \frac{(C_0 - C_t) \times V}{n} \tag{2}$$

where, q_t is the amount of FITC-lysozyme loaded in each SP ($\mu g\ SP^{-1}$) at a given time t, C_0 is the concentration of FITC-lysozyme in the stock solution ($mg\ mL^{-1}$), C_t is the concentration of FITC-lysozyme in the supernatant at time t ($mg\ mL^{-1}$), V is the volume of FITC-lysozyme solution added to the SPs (mL), and n is the number of SPs.

The loading capacity and efficiency of Si-SPs were determined by adding FITC-lysozyme solution at different concentrations to the six different types of SPs (with 5 Si-SPs per sample). The Si-SPs were sterilized with 100 μL of ethanol (80% v/v) at room temperature (~22 °C) for 4 h. The SPs were then washed with sterile Milli-Q water six times. Subsequently, 100 μL of FITC-lysozyme solution of different concentrations was added to the different types of Si-SPs. After loading the SPs for 3 days, 90 μL of the supernatant was withdrawn. The concentration of FITC-lysozyme in the supernatant was determined as previously described. The amount of FITC-lysozyme loaded in the different types of Si-SPs was calculated by subtracting the amount of FITC-

lysozyme in the supernatant from the amount of FITC-lysozyme in the original stock solution according to Equation 3:

$$q_t = \frac{(C_0 - C_n) \times V}{n} \tag{3}$$

where C_n is the concentration of FITC-lysozyme in the supernatant after 3 days (mg mL^{-1}).

The FITC-lysozyme loading efficiency was calculated from Equation 4:

$$\text{Loading efficiency (\%)} = \frac{m_0 - m_n}{m_0} \times 100\% \tag{4}$$

where m_0 is the total amount of FITC-lysozyme added to the SPs (µg) and m_n is the amount of free FITC-lysozyme in the supernatant.

In Vitro Release Studies. For the in vitro release studies, ^{L}Si-SPs and ^{L}Si-SPs^{alg} were examined. The FITC-lysozyme-loaded SPs for the in vitro release studies were prepared by sterilizing the SPs in 80% v/v ethanol as described above, followed by incubation of 10 SPs (^{L}Si-SPs or ^{L}Si-SPs^{alg}) in 100 µL of FITC-lysozyme solution (0.2 mg mL^{-1} in Milli-Q water)—these two types of SPs gave the highest drug loading. After 3 days of incubation, the supernatant was removed, and 100 µL of PBS (pH 7.4) was added to each tube and incubated at 37 °C. At defined time intervals (over 150 days), 90 µL of the solution was collected and replaced with fresh PBS. The fluorescence of the collected samples was measured with an Infinite M200 microplate reader, and the concentration of FITC-lysozyme in the supernatant was calculated using a standard curve of known concentrations of FITC-lysozyme (Figure S5a).

Drug release kinetics was also assessed after loading with higher quantities of the model drug FITC-lysozyme. A loading concentration of 1.0 mg mL^{-1} FITC-lysozyme (in Milli-Q water) was added to 10 ^{L}Si-SPs, and the in vitro drug release behavior of the SPs in PBS was assessed as described above using the standard curve in Figure S5b.

Additionally, the drug release kinetics of the SPs in a hydrogel, as a potential medium for surgical delivery, was assessed. Specifically, in vitro FITC-lysozyme release in PF127 hydrogel was examined using the same protocol as that described above. After 3 days of incubation with FITC-lysozyme, 33.3 µL of PF127 hydrogel (30 wt% in Milli-Q water) was added to a 1.7 mL centrifugation tube followed by addition of 16.7 µL of PBS buffer. PF127 hydrogel and PBS solution were kept in ice before use. The resulting concentration of PF127 was 20 wt%, which resulted in gelling as the solution was incubated at 37 °C.

For BDNF loading, 5 sterile ^{L}Si-SPs were incubated with 50 µL of BDNF solution (1.0 mg mL^{-1} in Milli-Q water). After 3 days of incubation, the supernatant was removed, and 100 µL of PBS (pH 7.4) was added to the tube and incubated at 37°C. At defined time intervals (over 40 days), 95 µL of the solution was collected and replaced with fresh 95 µL PBS for the duration of the release studies. The amount of BDNF released from ^{L}Si-SPs was determined using a BDNF-specific enzyme-linked immunosorbent assay (ELISA) and a standard curve of BDNF samples as per the manufacturer's protocol (Figure S6).

RESULTS AND DISCUSSION

Synthesis and Characterization of Silica Supraparticles. The electrospray setup illustrated in Scheme 1 (and Scheme S1) was used to prepare Si-SPs from a suspension of primary silica particles in alginate. The setup shows that as voltage is applied, liquid containing alginate and primary silica particles is ejected from the nozzle tip, forming a cone of liquid (i.e., a Taylor cone) from which spherical droplets emanate. The droplets are collected in a gelling bath of calcium chloride, which crosslinks the alginate to form spherical particles. A number of electrospray parameters can affect the assembly of the SPs, potentially impacting the final size and circularity of the assembled SPs, including nozzle diameter,[33] ionization mode of the electrospray,[34] and the

viscosity and the surface tension of the collection bath, as well as the five main parameters that were systematically varied in this study: (i) the concentration of alginate; (ii) the concentration of primary silica particles; (iii) the flow rate; (iv) the applied voltage; and (v) the distance to collector (distance between the nozzle tip and the surface of the calcium chloride). The size of the Si-SPs generated using variations in these five parameters are summarized in Table 1.

The viscosity of the solution, and potentially, its electrical conductivity and surface tension, was largely influenced by the concentration of alginate (Table 1, rows 1−3) and had a significant impact on Si-SPs formation.[33,35,36] At a relatively low alginate concentration (i.e. 5 mg mL^{-1}), nonspherical and small Si-SPs (<100 μm) were obtained, as the low viscosity of the alginate solution resulted in the formation of less stable droplets and transitioned between spraying and dripping.[37–39] When the concentration of alginate was increased to 30 mg mL^{-1}, the viscosity was relatively higher, and the synthesized Si-SPs were more spherical and larger (average diameter of ~550 μm) than those obtained using lower alginate concentrations.[33,40,41] When the alginate concentration was increased further, the viscosity was too high for the nozzle and syringe pump, and the system stalled or clogged. The diameter of the Si-SPs increased proportionally as the concentration of the primary silica particles increased (Table 1, rows 3−5). This direct correlation was expected as a large amount of silica in each droplet is expected to result in a large amount of silica remaining after calcination (i.e. after liquid and organic components are removed), compared with those obtained at lower concentrations of primary silica particles, where the lower mass fraction of silica results in large shrinkage during drying and calcination.

The influence of the applied voltage (between the nozzle and grounded calcium chloride bath) on the size of the Si-SPs was subsequently investigated (Table 1, rows 3, 6 and 7). At lower applied voltages and field strengths (i.e. 5 kV over 10 cm), the electric field force was too weak to form a

stable Taylor cone,[38,42,43] resulting in the formation of large droplets ("spitting" instead of "dripping"). When the applied voltage was increased from 5 to 13 kV and further to 21 kV, the diameter of the Si-SPs decreased significantly (from ~1500 to ~240 µm), as it transitioned from a dripping mode to an electrospray mode. Thus, a stronger electric field force is generated at higher applied voltages (13 and 21 kV), resulting in the formation of a more stable Taylor cone formation, and thus a well-controlled droplet generation (Scheme S1).[44,45]

The collector distance, which was varied from 4 to 15 cm, had little influence on the size of the Si-SPs, with the average diameter of the Si-SPs increasing slightly from ~560 to ~600 µm, (Table 1, rows 3, 8 and 9). This is consistent with previous studies by Bugarski et al.[46] and Goosen et al.,[47] which showed that the collector distance minimally influenced the diameter of alginate beads formed at high applied voltages (>12 kV) that are comparable with those used in our study).

Finally, the effect of the flow rate of the syringe pump on the formation of the Si-SPs was investigated (Table 1, rows 3, 10 and 11). As the flow rate was increased from 3 to 20 mL h^{-1}, there was negligible difference in particle size, with the average SP size shifting from ~540 to ~560 µm.

Table 1. Effect of Five Key Parameters on the Size of Si-SPs Assembled via Gel-Mediated Electrospray^a

	concentration of alginate (mg mL^{-1})	concentration of primary silica particles (mg mL^{-1})	voltage (kV)	collector distance (cm)	flow rate (mL h^{-1})	average SP diameter (µm)^b
1	5	40	13	10	8	<100
2	20	40	13	10	8	399 ± 87

17

3	30	40	13	10	8	544 ± 41
4	30	20	13	10	8	479 ± 38
5	30	50	13	10	8	759 ± 50
6	30	40	5	10	8	>1500
7	30	40	21	10	8	243 ± 31
8	30	40	13	4	8	563 ± 36
9	30	40	13	15	8	606 ± 62
10	30	40	13	10	3	545 ± 48
11	30	40	13	10	20	561 ± 57

[a]The Si-SPs reported in this table were prepared from primary silica particles with the large pores.

[b]The diameters of the Si-SPs reported herein were calculated after calcination of the Si-SPs[alg] and are shown as the mean diameter ± standard deviation obtained from analysis of at least 130 SPs.

Based on these results, Si-SPs prepared under the conditions presented in row 3 (Table 1), and which were used subsequently, were considered optimal as they resulted in spherical SPs with a diameter of approximately 550 μm (Figure 1a,b). For inner ear delivery, this is considered an ideal size as the SPs are large enough to potentially have high drug loading capacity, but small enough to be delivered via a cannula to the inner ear. The EISA method previously described for preparing Si-SPs can also lead to a versatile range of SPs in terms of size and circularity, but this would require extensive manual handling compared with the simple changes in electrospray parameters that are afforded by an automatable electrospray technique.

[L]Si-SPs were investigated in detail. From optical images of 130 particles, [L]Si-SPs had a diameter of 544 ± 41 μm (Figure S7a) and a spherical shape with a circularity of 0.854 ± 0.015 (Figure S7b). The three-dimensional (spherical) morphology of [L]Si-SPs was further confirmed using SEM at different tilted angles (Figure S8) and confocal laser scanning microscopy at various z heights (Figure S9). The surface of the Si-SPs was investigated by SEM (Figure 1c), and the results showed

that the primary silica particles were arranged in random order (e.g. in contrast to optical opal supraparticles[8]), and some spacing (void volume) between individual primary silica particles was apparent. Based on SEM analysis, there were negligible macroscopic differences between [L]Si-SPs, [S]Si-SPs, and [N]Si-SPs (Figure S10).
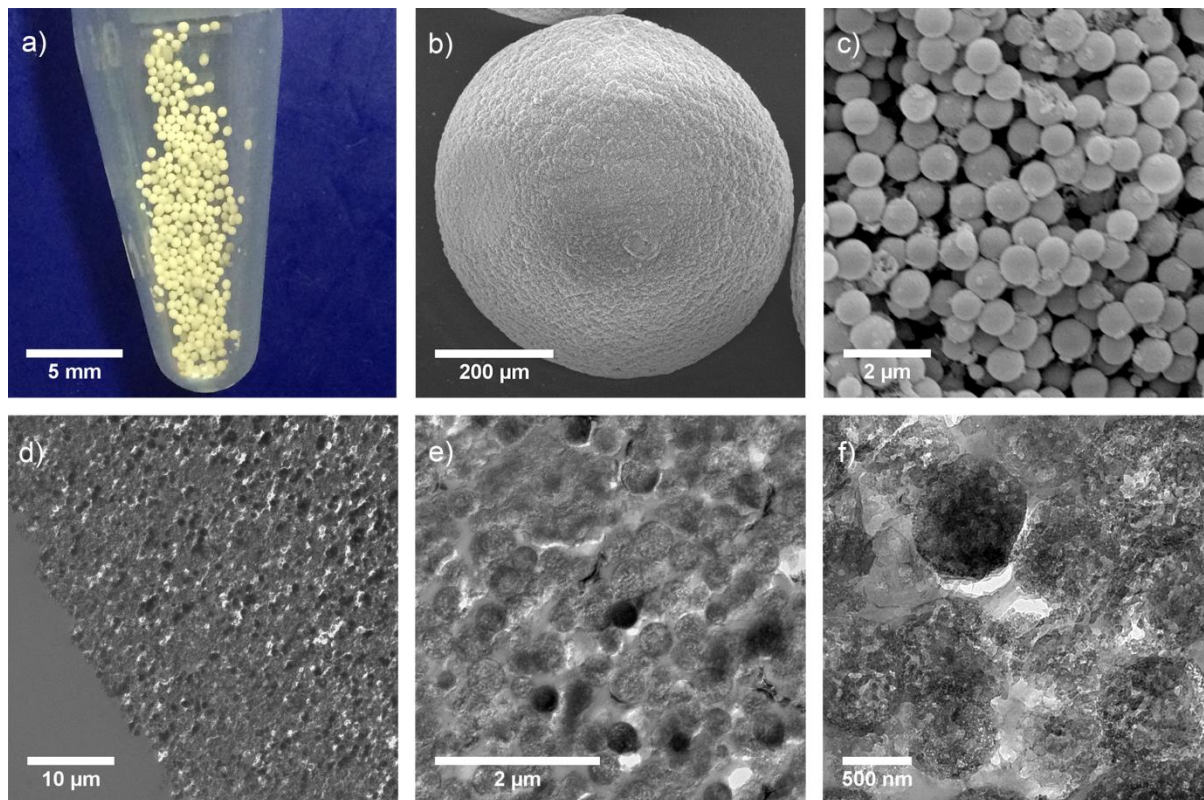

Figure 1. Characterization of [L]Si-SPs. (a) Photograph of [L]Si-SPs in a 1.7 mL centrifuge tube. (b) SEM image of a [L]Si-SP and (c) high-resolution SEM image showing the surface structure of a [L]Si-SP. (d–f) Cryo-electron tomograms (Cryo-ET) of [L]Si-SPs at different magnifications.

To investigate the inner structures of [L]Si-SPs, cryo-electron tomograms (cryo-ET) were also obtained (Figure 1d–f). The primary silica particles were closely packed, indicating that the Si-SPs are mechanically robust. This is consistent with the force–fracture testing shown in Figure S11—the average force required to fracture individual [L]Si-SP is 311 ± 93 mN.

SEM and TEM evaluation of the as-prepared primary silica particles with large pores both revealed the spherical morphology of the particles, with a diameter of 800–1000 nm (Figure 2a–c). For comparison, TEM images of nonporous primary silica particles and commercial primary silica particles with small pores are shown in Figure S12. Cryo-ET confirmed the porous structure of the primary particles with large pores and demonstrated the large porosity of the primary silica particles (Figure 2d). The Brunauer–Emmett–Teller (BET) method and Barrett–Joyner–Halenda (BJH) model were used to calculate the specific surface area and pore diameter distributions of the primary silica particles (Figure 2e), respectively. The specific surface area of the primary silica particles was 623 m^2 g^{-1} and they had a bimodal porous structure with smaller pores ranging from 2 to 3 nm and larger pores ranging from 15 to 64 nm. Note that from the cryo-ET image analysis (Figure 2d), many larger pores were also evident (>100 nm); the BJH technique primarily measures pores of <100 nm. This requirement also means that the porosity of the SPs and the void volume between individual primary particles cannot be measured accurately using N_2 adsorption–desorption technique. Nevertheless, the high porosity of the primary particles and the Si-SPs is expected to enable high drug loading capacity, which is a vital property for drug carriers aimed for sustained and long-term release.

X-ray photoelectron spectroscopy (XPS) was used to study the elemental composition of [L]Si-SPs (Figure S13a). High-resolution XPS spectra of the Si 2p region showed the presence of Si–O–Ca linkages (Figure S13b). These results suggest that upon calcination of [L]Si-SPs[alg], organic alginate is removed, but inorganic calcium remains. The calcination process also causes sintering and formation of Si–O–Si bonds.[21] Any residual calcium may be introduced into the Si–O–Si network, and thus, some Si–O–Ca–O–Si groups are also formed, which may confer additional robustness to the Si-SPs.
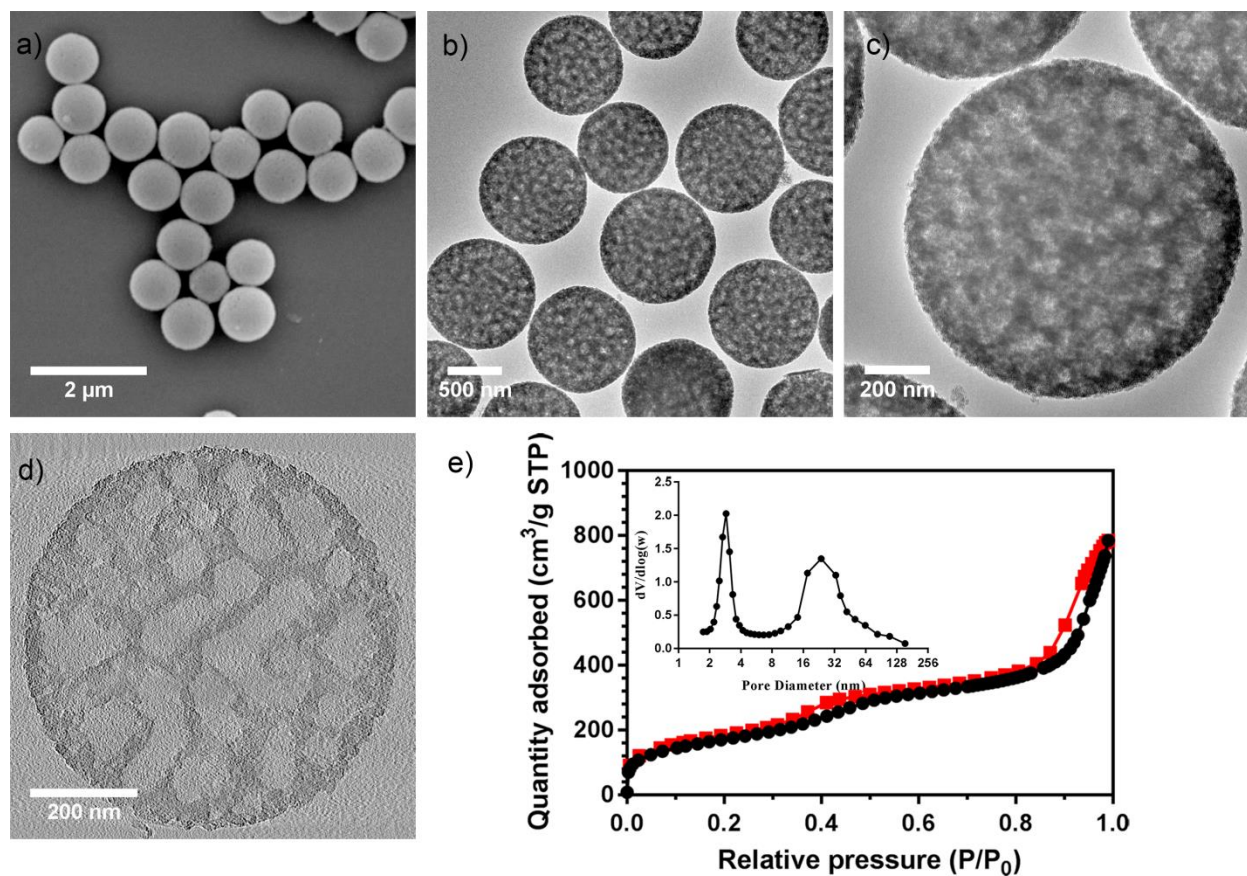
Figure 2. Characterization of primary silica particles with large pores. (a) SEM image of the primary silica particles. (b, c) TEM images of the primary silica particles at different magnifications. (d) Virtual slice through a primary silica particle by cryo-ET. (e) N_2 adsorption–desorption isotherm of the primary silica particles. Inset in (e) shows the distribution of the pores (<100 nm) of the primary silica particles.

In Vitro Cytotoxicity. To investigate the use of ^{L}Si-SPs as biocompatible drug carriers, in vitro cytotoxicity studies were performed. Human brain glioblastoma cells (U87MG cell line) were incubated with ^{L}Si-SPs, and cell viability was assessed using an Alamar Blue assay. As shown in Figure 3, ^{L}Si-SPs were nontoxic in this noncontact model even when the number of ^{L}Si-SPs was increased to 10 per well (1×10^4 cells per well). Typical in vivo treatment scenarios of similar particle systems suggest the administration of 1–8 SPs per inner ear.[20]
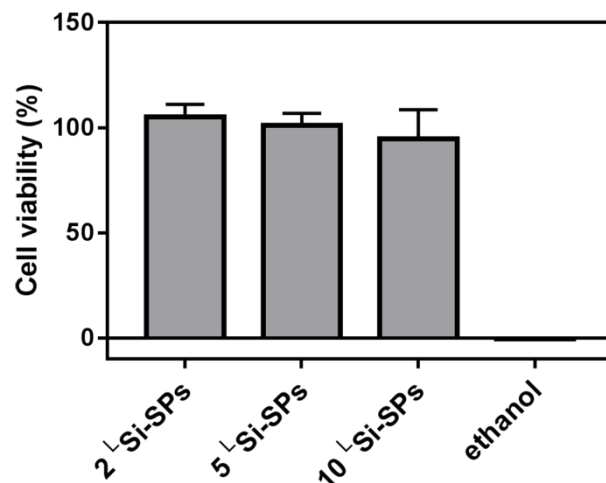
Figure 3. Cell viability of human brain glioblastoma cells (U87MG cell line) incubated with different numbers (2, 5, or 10) of ^{L}Si-SPs for 48 h. Ethanol added to cells with inserts was used as a negative (cytotoxic) control, and untreated cells represent 100% viability. The data presented are the average of four samples, and error bars represent standard deviations.

Drug Loading. To investigate the potential of Si-SPs, particularly ^{L}Si-SPs, as drug carriers for therapeutic proteins in biomedical applications, protein loading studies were conducted with model proteins. FITC-lysozyme was used as a model protein to mimic neurotrophin BDNF because of their similarities in their physicochemical properties (lysozyme, molecular weight (M_w) = 14.3 ± 0.5 kDa,[48] hydrodynamic radius (R_H) = 18.9 ± 0.25 Å,[48] and isoelectric point (pI) = 11;[49] BDNF, M_w = 13 kDa,[50] R_H = 24.0 ± 3.2 Å,[51] and pI = 10[50,52]). As shown in Figure 4, Si-SPs exhibited negative zeta potentials ranging from approximately −8 to −50 mV as the pH value increased from 4 to 10. Although ^{L}Si-SPs appear less negatively charged than ^{N}Si-SPs and ^{S}Si-SPs, perhaps because of their higher degree of porosity or the in-house method used to prepare the primary silica particles with large pores, positively charged lysozyme and BDNF are likely to be loaded into all Si-SPs, with electrostatic interactions playing a role in the process.
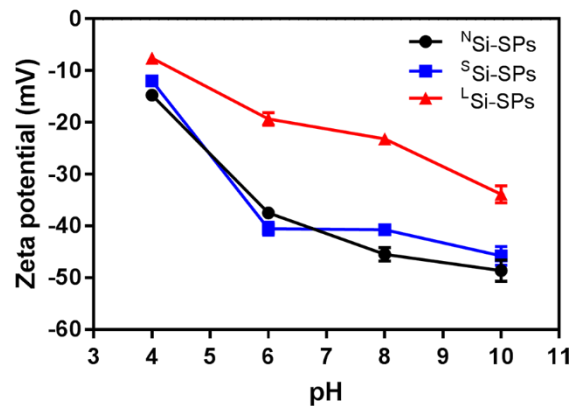
Figure 4. Zeta potential of ^{N}Si-SPs, ^{S}Si-SPs, and ^{L}Si-SPs as a function of pH. Zeta potential measurements were performed in 10 mM sodium acetate buffer (pH 4), 10 mM phosphate buffer (pH 6), 10 mM HEPES buffer (pH 8), and 10 mM sodium bicarbonate buffer (pH 10).

Confocal laser scanning microscopy (CLSM) images of the ^{L}Si-SPs (Figure 5a, b) indicated that FITC-lysozyme associated with the surface of ^{L}Si-SPs. However, as the ^{L}Si-SPs are quite large (hundreds of micrometers in diameter), standard confocal laser scanning microscopy is not ideally suited to imaging the internal structure of the SPs. Sectioning the ^{L}Si-SPs with a scalpel, however, allowed the internal structure of the SPs to be imaged. FITC-lysozyme was observed not only at the particle surface, but also within the porous internal structure of the ^{L}Si-SPs (Figure 5c).
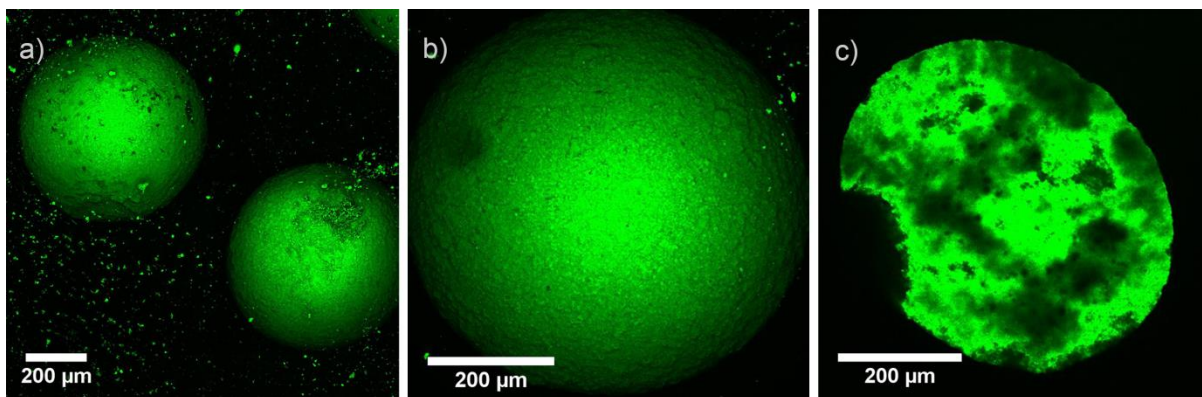
Figure 5. CLSM images of ^{L}Si-SP loaded with FITC-lysozyme (green). (a, b) CLSM images of ^{L}Si-SPs at different magnifications. (c) Interior of a fragmented ^{L}Si-SP loaded with FITC-lysozyme.
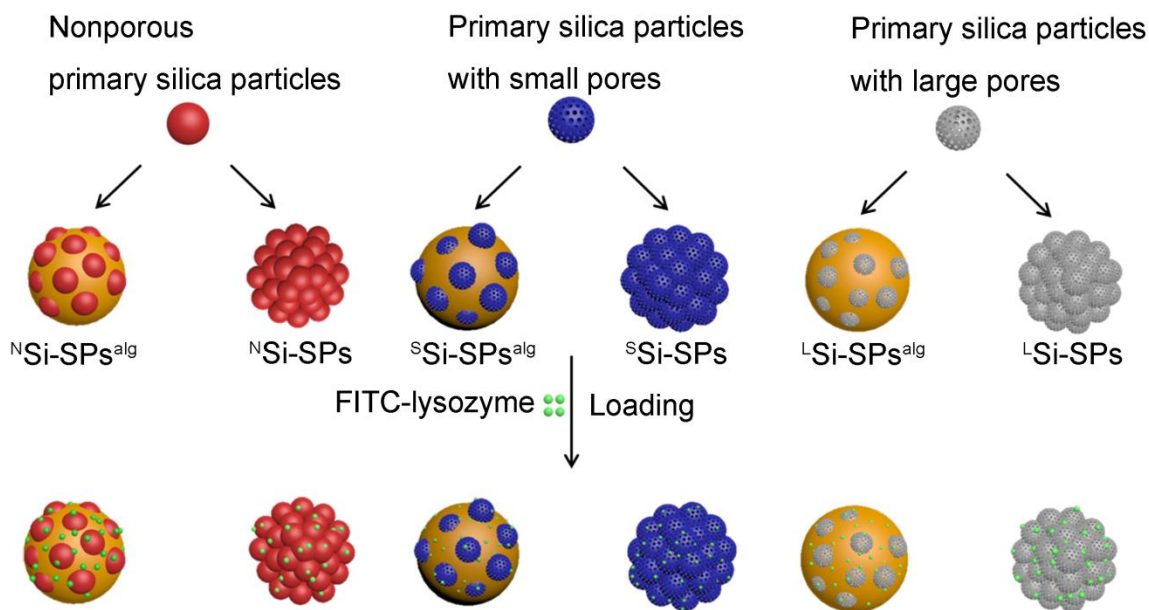
Scheme 2. Schematic illustration of FITC-lysozyme loading in six different types of Si-SPs: alginate/nonporous primary silica supraparticles (^{N}Si-SPs^{alg}); alginate/primary silica particles with small pores supraparticles (^{S}Si-SPs^{alg}); alginate/primary silica particles with large pore supraparticles (^{L}Si-SPs^{alg}); silica supraparticles prepared from nonporous primary silica particles (^{N}Si-SPs); silica supraparticles prepared from primary silica particles with small pores (^{S}Si-SPs); and silica supraparticles prepared from primary silica particles with large pores (^{L}Si-SPs).

Determination of Drug Loading Kinetics, Capacity, and Efficiency. Incubation of lysozyme or neurotrophins with Si-SPs results in protein-loaded Si-SPs. As this process depends on several parameters (including incubation time and drug loading concentration), drug loading kinetics was evaluated across a series of loading conditions.[53] Drug loading kinetic data were generated for six

different types of SPs (^{N}Si-SPs^{alg}, ^{S}Si-SPs^{alg}, ^{L}Si-SPs^{alg}, ^{N}Si-SPs, ^{S}Si-SPs, and ^{L}Si-SPs) (Scheme 2). Figure 6 shows the effect of incubation time on FITC-lysozyme loading for the different types of SPs studied. Drug loading is reported as mass of protein per SP; ^{L}Si-SPs have an average weight of 50 μg, whereas ^{L}Si-SPs^{alg} have an average weight of 95 μg. Incubation of FITC-lysozyme with ^{N}Si-SPs^{alg} and ^{S}Si-SPs^{alg} appeared to reach equilibration after 48 h, whereas saturation of the ^{L}Si-SPs^{alg} with FITC-lysozyme took longer (~96 h) (Figure 6a). In contrast, the drug loading time required to approach saturation for both ^{N}Si-SPs and ^{S}Si-SPs was ~24 h, whereas that for ^{L}Si-SPs was ~48 h. In summary, both ^{L}Si-SPs and ^{L}Si-SPs^{alg} required longer loading times to approach saturation, but could load more FITC-lysozyme than the other types of Si-SPs.
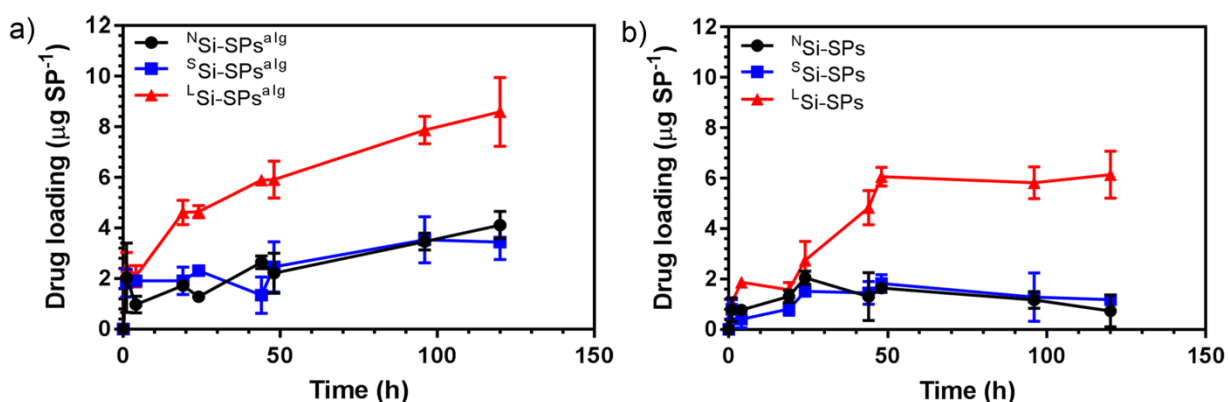
Figure 6. Drug loading kinetics of the different types of Si-SPs prepared. Effect of incubation time on FITC-lysozyme (0.6 mg mL^{-1} in Milli-Q water) loaded into (a) ^{N}Si-SPs^{alg}, ^{S}Si-SPs^{alg}, and ^{L}Si-SPs^{alg}, and (b) ^{N}Si-SPs, ^{S}Si-SPs, and ^{L}Si-SPs. The data are shown as the average of three replicates, each using 5 SPs, and error bars represent standard deviations.

Based on the results obtained above (Figure 6), an incubation time of 3 days was used in subsequent experiments. Specifically, the loading capacity for the different types of SPs was investigated after a 3-day incubation period with FITC-lysozyme at different loading concentrations (in Milli-Q water) (Figure 7). In general, as the concentration of FITC-lysozyme

increased, drug loading increased. Additionally, the alginate-containing Si-SPs ([N]Si-SPs[alg], [S]Si-SPs[alg], and [L]Si-SPs[alg]) had higher loading capacities than the alginate-removed Si-SPs ([N]Si-SPs, [S]Si-SPs and [L]Si-SPs) at a given FITC-lysozyme concentration. This is likely due to increased electrostatic interactions between positively charged FITC-lysozyme and negatively charged alginate around neutral pH value.[24] At low FITC-lysozyme loading concentrations (<0.4 mg mL^{-1}), [L]Si-SPs[alg] had a similar drug loading capacity to [N]Si-SPs[alg] and [S]Si-SPs[alg]. In contrast, when the drug loading concentration was higher (>0.4 mg mL^{-1}), a higher amount of FITC-lysozyme could be loaded into [L]Si-SPs[alg] when compared with that achieved for [N]Si-SPs[alg] and [S]Si-SPs[alg]. For the alginate-removed Si-SPs, a similar trend was observed: [L]Si-SPs could load more FITC-lysozyme than [N]Si-SPs and [S]Si-SPs. These results suggest that the large porous structures in [L]Si-SPs and [L]Si-SPs[alg] are key factors to improving drug loading, likely by providing additional surface areas of contact and hence loading and capacity when outer particle surfaces and intra-particle areas (in the SP structures) have been fully saturated with protein.

The experimentally determined maximum loading capacities of FITC-lysozyme into [N]Si-SPs[alg] and [S]Si-SPs[alg] were ~3 and 2 µg SP^{-1}, respectively. These values were significantly lower than that observed for [L]Si-SPs[alg] i.e., 15 µg SP^{-1} (initial FITC-lysozyme concentration was 1.5 mg mL^{-1} and loading time was 3 days). The experimentally determined maximum loading capacities of FITC-lysozyme into [N]Si-SPs and [S]Si-SPs were ~2 and 1 µg SP^{-1} respectively, which were also significantly lower than that achieved for [L]Si-SPs i.e., ~10 µg SP^{-1} (initial FITC-lysozyme concentration was 5.0 mg mL^{-1} and loading time was 3 days). The reason for using this higher concentration of FITC-lysozyme for [L]Si-SPs[alg] and [L]Si-SPs—compared to [N]Si-SPs[alg], [S]Si-SPs[alg], [N]Si-SPs, and [S]Si-SPs—was that [L]Si-SPs[alg] and [L]Si-SPs were not reaching drug loading saturation using the lower concentration. The loading capacity per SP also depends on the diameter of [L]Si-

SPs where larger [L]Si-SPs (1000 μm) displayed higher loading capacities than the smaller [L]Si-SPs (200 μm) counterparts after 3 days incubation with FITC-lysozyme (Figure S14). This further supports the conclusion that a larger surface area, as a result of both a larger SP diameter and increased porosity, leads to a higher protein loading on the silica surface.

The drug loading efficiency of the six different SPs is summarized in Figure 7c and 7d. As the loading concentration of FITC-lysozyme increased, greater quantities of FITC-lysozyme could be loaded into SPs. However, overall, the efficiency of loading decreased with increasing FITC-lysozyme concentration.
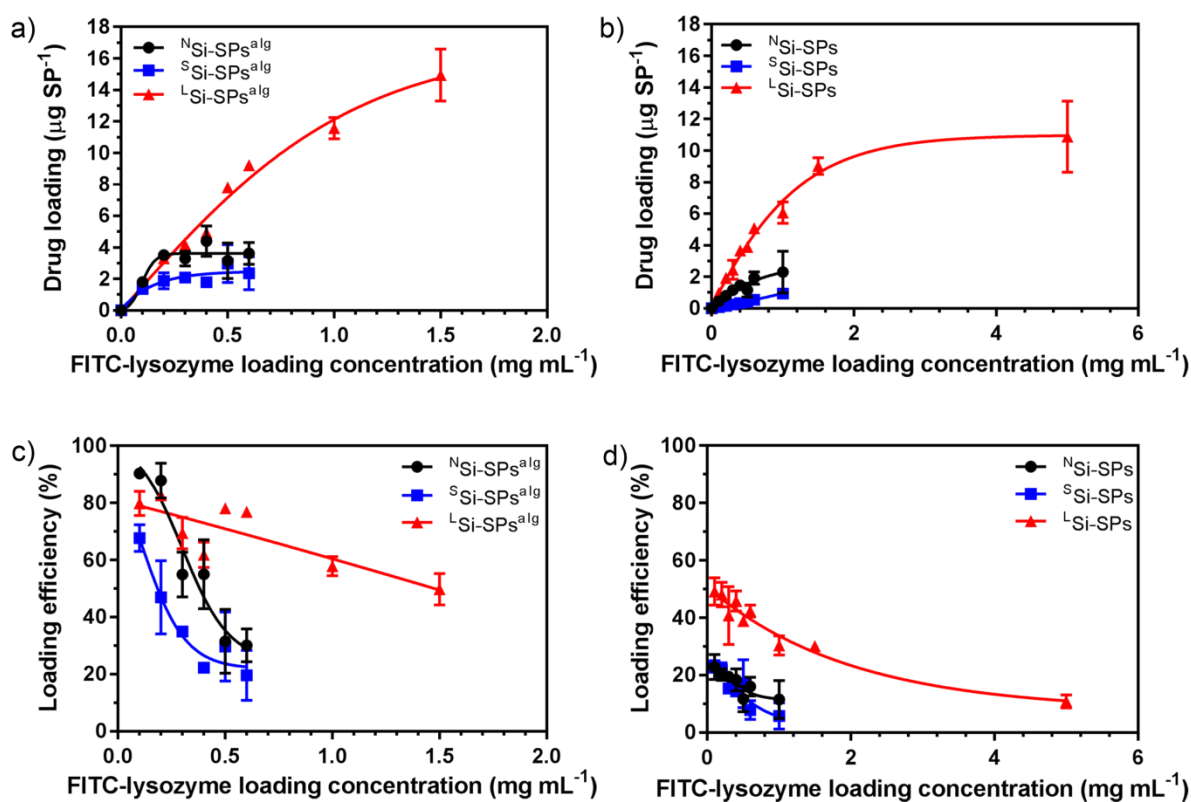
Figure 7. Loading of Si-SPs with FITC-lysozyme at different loading concentrations following a 3-day incubation period. (a) Amount of FITC-lysozyme loaded into Si-SPs[alg] as a function of FITC-lysozyme loading concentration. (b) Amount of FITC-lysozyme loaded into Si-SPs as a

27

function of FITC-lysozyme loading concentration. The relationship between drug loading and FITC-lysozyme loading concentration from 0 to 1.0 mg mL^{-1} is shown in Figure S15. FITC-lysozyme loading efficiency of (c) Si-SPs^{alg} and (d) Si-SPs. Data presented are averages of three replicates, each using 5 SPs, and error bars represent standard deviations.

Drug Release. For the release studies, 10 ^{L}Si-SPs or 10 ^{L}Si-SPs^{alg} were incubated in PBS (pH 7.4) at 37 °C. The Si-SPs were initially incubated for 3 days with FITC-lysozyme at a loading concentration of 0.2 mg mL^{-1}. The FITC-lysozyme loading values were 1.89 ± 0.02 and 1.93 ± 0.01 µg SP^{-1} for ^{L}Si-SPs and ^{L}Si-SPs^{alg}, respectively.

As shown in Figure 8a, >1 µg of FITC-lysozyme was released per ^{L}Si-SP over a period of more 150 days, with 50% of the protein adsorbed being released at ~80 days as indicated by first-order release kinetics model in Figure S16. A lower amount of FITC-lysozyme (~0.4 µg per SP) was released from ^{L}Si-SPs^{alg} over the 150-day period. The lower release exhibited by the alginate/silica SPs may indicate blockage of the large pores of the primary silica particles by alginate[54] or potentially strong interaction between alginate and lysozyme, thereby preventing or retarding lysozyme release. The measured amounts of FITC-lysozyme released at each time point (which were used to prepare the cumulative results presented in Figure 8) are shown in Figure S17.

The FITC-lysozyme and BDNF release profiles from ^{L}Si-SPs were also investigated at a higher incubation concentration (1.0 mg mL^{-1}). The amounts of FITC-lysozyme and BDNF respectively loaded at this loading concentration were 6.49 ± 0.48 and 7.17 µg SP^{-1}, respectively. Under this higher concentration loading condition, the release profile for FITC-lysozyme was biphasic. A burst release period was apparent in the first 3 days, followed by sustained release over more than 110 days (Figure 8b). Approximately 4.2 µg FITC-lysozyme was released per SP in the burst stage. After 3 days, ~2.3 µg FITC-lysozyme remained loaded in the SPs, and a more sustained release

behavior was subsequently observed. The slower kinetics of release overall compared with protein loading relates to the strong electrostatic interaction between the silica and lysozyme or BDNF that hinders the release of the protein. The protein is slowly released under physiological conditions (in PBS, at 37 °C), as the PBS disrupts the electrostatic interactions and free protein diffuses out of the porous particle. The amounts of FITC-lysozyme released at each time point were approximately 0.07 to 4 µg per SP (Figure S18). As shown in Figure 8c, the in vitro BDNF release profile was similar to that of FITC-lysozyme, with a burst release observed in the first 3 days followed by a more sustained release for over 40 days. The amounts of BDNF released at each time point again ranged from approximately 0.1 to 3 µg per SP (Figure S19). The cumulative released value of the SPs after 40 days was ~4.68 µg of drug, and the weight of each SP was ~0.05 mg. Thus, the observed cumulative release was about 93.6 µg mg^{-1}. Interestingly, this is a 4000-fold improvement compared to what has recently been observed for nanoporous silica nanoparticles,[55] further highlighting the large difference between individual porous nanoparticles and supraparticle assemblies. The amount of BDNF released was also measured by a Micro BCA assay (Figure S20), and similar results were obtained. The released BDNF is expected to be biologically active, as shown in our previous work that described the implantation of BDNF-loaded Si-SPs (prepared using EISA) in the inner ear of guinea pigs.[20,21]
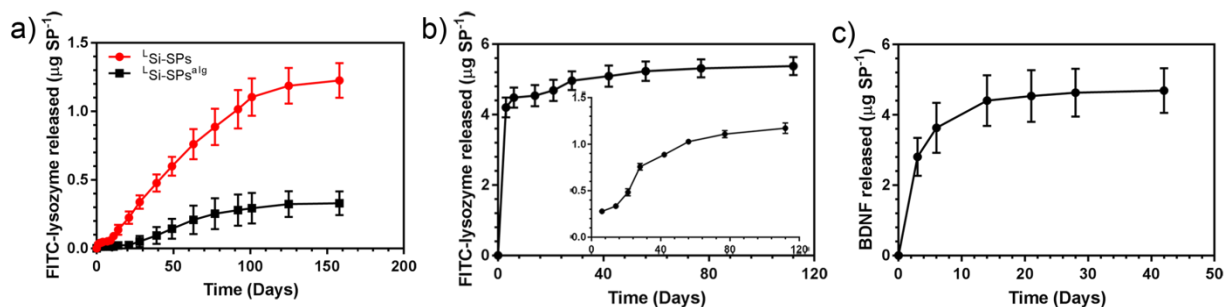
Figure 8. In vitro cumulative drug release profiles. (a). In vitro FITC-lysozyme (loading concentration 0.2 mg mL^{-1}, drug loading for 3 days) release from ^{L}Si-SPs and ^{L}Si-SPs^{alg}. (b) In vitro FITC-lysozyme (loading concentration 1.0 mg mL^{-1}, drug loading for 3 days) release from ^{L}Si-SPs. Inset in (b) shows the in vitro FITC-lysozyme release profile starting from Day 6. (c) In vitro BDNF release from ^{L}Si-SPs (loading concentration 1.0 mg mL^{-1}, drug loading for 3 days). BDNF ELISA (Abcam) was used for measuring the BDNF concentration. Data presented in (a)–(c) are averages of three replicates, each using 10 SPs in (a) and (b) and 1 SP in (c), and error bars represent standard deviations. Release data for individual time points (non-cumulative) are available in Figures S17–S19.

To investigate potential methods to further tune drug release behaviors and aid surgical delivery to the inner ear, in vitro drug release studies of ^{L}Si-SPs and ^{L}Si-SPs^{alg} incorporated within PF127 hydrogels were performed. PF127 hydrogels form viscous liquids at cold temperatures (e.g. 4 °C) and gel at body temperature (37 °C).[56] The results showed that most of the FITC-lysozyme was released from both ^{L}Si-SPs and ^{L}Si-SPs^{alg} that were incorporated within PF127 hydrogel by Day 14 (Figure S21), indicating accelerated release kinetics when compared with the drug release behaviors of Si-SPs that were not incorporated within the PF127 hydrogel (Figure 8). This accelerated release rate might be attributed to the surfactant properties of PF127. PF127 is an amphiphilic block copolymer of polypropylene oxide and polyethylene oxide, which can both reduce interfacial tension and form micellar structures upon dilution. These properties may facilitate desorption and release of loaded proteins. The supraparticle–PF127 system is therefore more suitable when shorter-term drug release is desired (~1 week), whereas the PF127-free supraparticle systems are more suitable for longer-term (several months) drug release.

Porous silica particles can be degraded in biological environments into silicic acid, which can be excreted into the urine, and are of interest for diverse biomedical applications.[57] To investigate the degradation behaviors of our system, [L]Si-SPs were incubated in PBS for 150 days (pH 7.4, 37 °C) (Figure 9). The diameter of the [L]Si-SPs decreased by ~55%, and the shape/morphology of the [L]Si-SPs changed substantially. The primary silica particles on the surface of the [L]Si-SPs also changed in both morphology and size (cf. Figures 1 and 9).
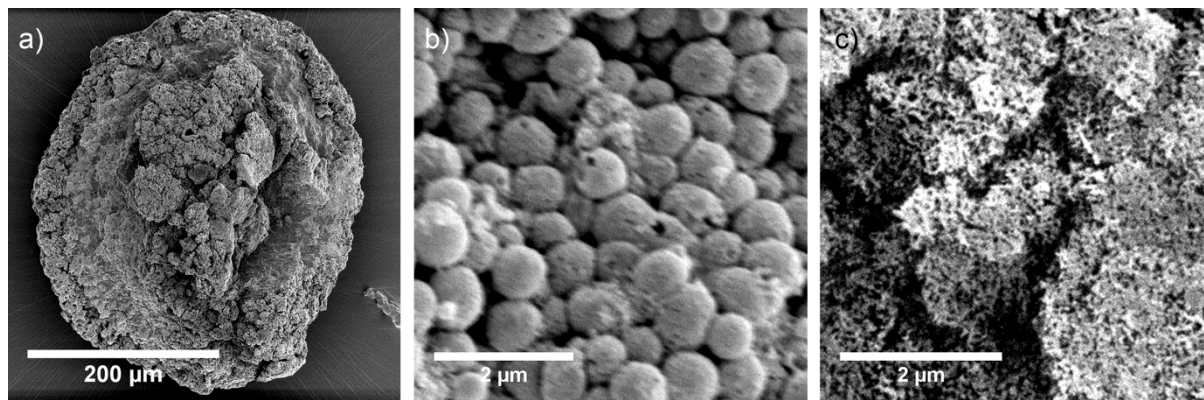
Figure 9. Degradation of [L]Si-SPs after 150 days of in vitro drug release studies. (a) SEM image of [L]Si-SPs after 150 days of incubation in PBS (pH 7.4) at 37 °C. (b, c) SEM images of the surface structure of [L]Si-SPs after 150 days of incubation in PBS (pH 7.4) at 37 °C.

CONCLUSIONS

Herein, we presented a rapid and automatable electrospray technique to prepare SPs based on an alginate hydrogel-mediated approach. Thousands of SPs could be prepared within 30 min, which otherwise would take weeks using conventional EISA approach. The generated SPs were spherical and showed good reproducibility with respect to size and shape. Si-SPs with different sizes were fabricated by adjusting five main system variables including sample composition and instrumental parameters. Six different SPs were prepared, and among these, [L]Si-SPs showed the highest

capability to load therapeutically relevant levels of neurotrophin (10 µg SP^{-1} when loaded for 3 days with 5.0 mg mL^{-1} FITC-lysozyme or 7.17 µg SP^{-1} when loaded for 3 days with 1.0 mg mL^{-1} BDNF). In vitro release profiles demonstrated sustained release of FITC-lysozyme over a period of more than 110 days and BDNF over more than 40 days, as well as a burst release stage (which may provide a loading dose) for both drugs in the first 3 days. ^{L}Si-SPs, loaded using lower drug loading concentrations (1.89 µg SP^{-1} when loaded for 3 days with 0.2 mg mL^{-1} FITC-lysozyme) also exhibited sustained drug release for more than 150 days. Interestingly, the cumulative release from the supraparticles after 40 days was around 94 µg mg^{-1}, a 4000-fold improvement compared with recently reported nanoporous silica nanoparticles.[52] The release kinetics of the supraparticles could be further tuned via the combined use of ^{L}Si-SPs in block co-polymer-based hydrogels. These findings show that ^{L}Si-SPs assembled through gel-mediated electrospray are promising drug carriers for therapies that require long-term delivery of protein drugs such as for the treatment of inner ear diseases.

ASSOCIATED CONTENT

Supporting Information. Scheme of crosslinking between calcium chloride and alginate; summary of the six different types of supraparticles examined in the drug loading kinetics, capacity, and efficiency studies; photographs of the electrospray setup and force–fracture test machine; optical microscopy images of alginate/silica supraparticles; SEM images of ^{L}Si-SPs at different tilted angles; SEM images of ^{N}Si-SPs and ^{S}Si-SPs; TEM images of nonporous primary silica particles and primary silica particles with small pores; calibration curves for FITC-lysozyme and BDNF concentration determination; confocal laser scanning microscopy images of ^{L}Si-SPs at various thicknesses; size distribution and circularity of ^{L}Si-SPs; XPS analysis of ^{L}Si-SPs; FITC-lysozyme loading and release curves of ^{L}Si-SPs with different diameters; drug loading capacity of

SPs as a function of drug loading concentration; amounts of FITC-lysozyme and BDNF released from ^{L}Si-SPs at given time points; first-order release kinetics of FITC-lysozyme and BDNF release from ^{L}Si-SPs; BDNF concentration determination using Micro BCA assay; in vitro FITC-lysozyme release data of Si-SPs–PF127 hydrogel system.

AUTHOR INFORMATION

Corresponding author

*E-mail: fcaruso@unimelb.edu.au

Notes

The authors have filed a patent containing some of the findings reported herein. The authors declare no other competing financial interests.

ACKNOWLEDGMENT

REFERENCES

(1) Xia, Y.; Yin, Y.; Lu, Y.; McLellan, J. Template-Assisted Self-Assembly of Spherical Colloids into Complex and Controllable Structures. *Adv. Funct. Mater.* **2003**, *13*, 907–918.

(2) Lu, Z.; Yin, Y. Colloidal Nanoparticle Clusters: Functional Materials by Design. *Chem. Soc. Rev.* **2012**, *41*, 6874–6887.

(3) Dai, Q.; Bertleff-Zieschang, N.; Braunger, J. A.; Björnmalm, M.; Cortez-Jugo, C.; Caruso, F. Particle Targeting in Complex Biological Media. *Adv. Healthcare Mater.* **2017**, *7*, 1700575.

(4) Cui, J.; Richardson, J. J.; Björnmalm, M.; Faria, M.; Caruso, F. Nanoengineered Templated Polymer Particles: Navigating the Biological Realm. *Acc. Chem. Res.* **2016**, *49*, 1139–1148.

(5) Sperling, M.; Gradzielski, M. Droplets, Evaporation and a Superhydrophobic Surface: Simple Tools for Guiding Colloidal Particles into Complex Materials. *Gels* **2017**, *3*, 15.

(6) Lu, Z.; Gao, C.; Zhang, Q.; Chi, M.; Howe, J. Y.; Yin, Y. Direct Assembly of Hydrophobic Nanoparticles to Multifunctional Structures. *Nano Lett.* **2011**, *11*, 3404–3412.

(7) Phillips, K. R.; England, G. T.; Sunny, S.; Shirman, E.; Shirman, T.; Vogel, N.; Aizenberg, J. A Colloidoscope of Colloid-Based Porous Materials and Their Uses. *Chem. Soc. Rev.* **2016**, *45*, 281–322.

(8) Rastogi, V.; Melle, S.; Calderon, O. G.; García, A. A.; Marquez, M.; Velev, O. D. Synthesis of Light-Diffracting Assemblies from Microspheres and Nanoparticles in Droplets on a Superhydrophobic Surface. *Adv. Mater.* **2008**, *20*, 4263–4268.

(9) Yeo, S. J.; Tu, F.; Kim, S. H.; Yi, G. R.; Yoo, P. J.; Lee, D. Angle- and Strain-Independent Coloured Free-Standing Films Incorporating Non-Spherical Colloidal Photonic Crystals. *Soft Matter* **2015**, *11*, 1582–1588.

(10) Rastogi, V.; Velev, O. D. Development and Evaluation of Realistic Microbioassays in Freely Suspended Droplets on a Chip. *Biomicrofluidics* **2007**, *1*, 014107.

(11) Xu, S.; Weng, Z.; Tan, J.; Guo, J.; Wang, C. Hierarchically Structured Porous Organic Polymer Microspheres with Built-in Fe_3O_4 Supraparticles: Construction of Dual-Level Pores for Pt-Catalyzed Enantioselective Hydrogenation. *Polym. Chem.* **2015**, *6*, 2892–2899.

(12) Gao, W.; Wang, J. The Environmental Impact of Micro/Nanomachines: A Review. *ACS Nano* **2014**, *8*, 3170–3180.

(13) Rastogi, V.; Velikov, K. P.; Velev, O. D. Microfluidic Characterization of Sustained Solute Release from Porous Supraparticles. *Phys. Chem. Chem. Phys.* **2010**, *12*, 11975–11983.

(14) Ma, W. F.; Wu, K. Y.; Tang, J.; Li, D.; Wei, C.; Guo, J.; Wang, S. L.; Wang, C. C. Magnetic Drug Carrier with a Smart pH-Responsive Polymer Network Shell for Controlled Delivery of Doxorubicin. *J. Mater. Chem.* **2012**, *22*, 15206–15214.

(15) Farinas, I.; Jones, K. R.; Tessarollo, L.; Vigers, A. J.; Huang, E.; Kirstein, M.; de Caprona, D. C.; Coppola, V.; Backus, C.; Reichardt, L. F.; Fritzsch, B. Spatial Shaping of Cochlear Innervation by Temporally Regulated Neurotrophin Expression. *J. Neurosci.* **2001**, *21*, 6170–6180.

(16) Khalin, I.; Alyautdin, R.; Kocherga, G.; Bakar, M. A. Targeted Delivery of Brain-Derived Neurotrophic Factor for the Treatment of Blindness and Deafness. *Int. J. Nanomed.* **2015**, *10*, 3245–3267.

(17) Wise, A. K.; Gillespie, L. N. Drug Delivery to the Inner Ear. *J. Neural Eng.* **2012**, *9*, 065002.

(18) Kho, S. T.; Pettis, R. M.; Mhatre, A. N.; Lalwani, A. K. Safety of Adeno-Associated Virus as Cochlear Gene Transfer Vector: Analysis of Distant Spread Beyond Injected Cochleae. *Mol. Ther.* **2000**, *2*, 368–373.

(19) Zhang, X.; Chen, G.; Wen, L.; Yang, F.; Shao, A. L.; Li, X.; Long, W.; Mu, L. Novel Multiple Agents Loaded PLGA Nanoparticles for Brain Delivery via Inner Ear Administration: In Vitro and in Vivo Evaluation. *Eur. J. Pharm. Sci.* **2013**, *48*, 595–603.

(20) Wise, A. K.; Tan, J.; Wang, Y.; Caruso, F.; Shepherd, R. K. Improved Auditory Nerve Survival with Nanoengineered Supraparticles for Neurotrophin Delivery into the Deafened Cochlea. *PLoS One* **2016**, *11*, e0164867.

(21) Wang, Y.; Wise, A. K.; Tan, J.; Maina, J. W.; Shepherd, R. K.; Caruso, F. Mesoporous Silica Supraparticles for Sustained Inner-Ear Drug Delivery. *Small* **2014**, *10*, 4244–4248.

(22) Maina, J. W.; Cui, J.; Björnmalm, M.; Wise, A. K.; Shepherd, R. K.; Caruso, F. Mold-Templated Inorganic–Organic Hybrid Supraparticles for Codelivery of Drugs. *Biomacromolecules* **2014**, *15*, 4146–4151.

(23) Lee, K. Y.; Mooney, D. J. Alginate: Properties and Biomedical Applications. *Prog. Polym. Sci.* **2012**, *37*, 106–126.

(24) Li, M.; Elder, T.; Buschle-Diller, G. Alginate-Based Polysaccharide Beads for Cationic Contaminant Sorption from Water. *Polym. Bull.* **2017**, *74*, 1267–1281.

(25) Gombotz, W. R.; Wee, S. F. Protein Release from Alginate Matrices. *Adv. Drug Delivery Rev.* **2012**, *64*, 194–205.

(26) Nedović, V. A.; Obradović, B.; Leskošek-Čukalović, I.; Trifunović, O.; Pešić, R.; Bugarski, B. Electrostatic Generation of Alginate Microbeads Loaded with Brewing Yeast. *Process Biochem.* **2001**, *37*, 17–22.

(27) Sridhar, R.; Ramakrishna, S. Electrosprayed Nanoparticles for Drug Delivery and Pharmaceutical Applications. *Biomatter* **2013**, *3*, e24281.

(28) Zhang, L.; Huang, J.; Si, T.; Xu, R. X. Coaxial Electrospray of Microparticles and Nanoparticles for Biomedical Applications. *Expert Rev. Med. Devices* **2012**, *9*, 595–612.

(29) Cui, J.; De Rose, R.; Alt, K.; Alcantara, S.; Paterson, B. M.; Liang, K.; Hu, M.; Richardson, J. J.; Yan, Y.; Jeffery, C. M.; Price, R. I.; Peter, K.; Hagemeyer, C. E.; Donnelly, P. S.; Kent, S. J.; Caruso, F. Engineering Poly(ethylene glycol) Particles for Improved Biodistribution. *ACS Nano* **2015**, *9*, 1571–1580.

(30) Kremer, J. R.; Mastronarde, D. N.; McIntosh, J. R. Computer Visualization of Three-Dimensional Image Data Using Imod. *J. Struct. Biol.* **1996**, *116*, 71–76.

(31) Anderson, S. L.; Luber, E. J.; Olsen, B. C.; Buriak, J. M. Substance over Subjectivity: Moving Beyond the Histogram. *Chem. Mater.* **2016**, *28*, 5973–5975.

(32) Hiramatsu, M.; Okabe, N.; Tomita, K. Preparation and Properties of Lysozyme Modified by Fluorescein-Isothiocyanate. *J. Biochem.* **1973**, *73*, 971–978.

(33) Moghadam, H.; Samimi, M.; Samimi, A.; Khorram, M. Electro-Spray of High Viscous Liquids for Producing Mono-Sized Spherical Alginate Beads. *Particuology* **2008**, *6*, 271–275.

(34) Faizal, F.; Saallah, S.; Lenggoro, I. W. Particulate Structures Produced by Electrosprays of Colloidal Silica Suspensions in Both Negative and Positive Zeta Potentials. *Adv. Powder Technol.* **2018**, *29*, 1771–1777.

(35) Desai, S.; Harrison, B. In *Printed Biomaterials: Novel Processing and Modeling Techniques for Medicine and Surgery*; Narayan, R.; Boland, T.; Yuan-Shin, L., Eds.: Springer: New York, USA, 2009; Chapter 5, pp 76–77.

(36) Moghadam, H.; Samimi, M.; Samimi, A.; Khorram, M. Electrospray Modeling of Highly Viscous and Non-Newtonian Liquids. *J. Appl. Polym. Sci.* **2010**, *118*, 1288–1296.

(37) Davarcı, F.; Turan, D.; Ozcelik, B.; Poncelet, D. The Influence of Solution Viscosities and Surface Tension on Calcium-Alginate Microbead Formation Using Dripping Technique. *Food Hydrocolloids* **2017**, *62*, 119–127.

(38) Tapia-Hernandez, J. A.; Torres-Chavez, P. I.; Ramirez-Wong, B.; Rascon-Chu, A.; Plascencia-Jatomea, M.; Barreras-Urbina, C. G.; Rangel-Vazquez, N. A.; Rodriguez-Felix, F. Micro-and Nanoparticles by Electrospray: Advances and Applications in Foods. *J. Agric. Food Chem.* **2015**, *63*, 4699–4707.

(39) Liao, Y. T.; Wu, K. C.; Yu, J. Synthesis of Mesoporous Silica Nanoparticle-Encapsulated Alginate Microparticles for Sustained Release and Targeting Therapy. *J. Biomed. Mater. Res., Part B* **2014**, *102*, 293–302.

(40) Badwan, A.; Abumalooh, A.; Sallam, E.; Abukalaf, A.; Jawan, O. A Sustained Release Drug Delivery System Using Calcium Alginate Beads. *Drug Dev. Ind. Pharm.* **1985**, *11*, 239–256.

(41) Lotfipour, F.; Mirzaeei, S.; Maghsoodi, M. Evaluation of the Effect of $CaCl_2$ and Alginate Concentrations and Hardening Time on the Characteristics of *Lactobacillus Acidophilus* Loaded Alginate Beads Using Response Surface Analysis. *Adv. Pharm. Bull.* **2012**, *2*, 71–78.

(42) Khorram, M.; Samimi, M.; Samimi, A.; Moghadam, H. Electrospray Preparation of Propranolol-Loaded Alginate Beads: Effect of Matrix Reinforcement on Loading and Release Profile. *J. Appl. Polym. Sci.* **2015**, *132*, 41334.

(43) Moghadam, H.; Samimi, M.; Samimi, A.; Khorram, M. Study of Parameters Affecting Size Distribution of Beads Produced from Electro-Spray of High Viscous Liquids. *Iran. J. Chem. Eng.* **2009**, *6*, 88–98.

(44) Chakraborty, S.; Liao, I. C.; Adler, A.; Leong, K. W. Electrohydrodynamics: A Facile Technique to Fabricate Drug Delivery Systems. *Adv. Drug Delivery Rev.* **2009**, *61*, 1043–1054.

(45) Coll, A.; Bermejo, S.; Hernandez, D.; Castaner, L. Colloidal Crystals by Electrospraying Polystyrene Nanofluids. *Nanoscale Res. Lett.* **2013**, *8*, 26.

(46) Bugarski, B.; Li, Q.; Goosen, M. F.; Poncelet, D.; Neufeld, R. J.; Vunjak, G. Electrostatic Droplet Generation: Mechanism of Polymer Droplet Formation. *AlChE J.* **1994**, *40*, 1026–1031.

(47) Goosen, M. F.; Al-Ghafri, A. S.; Mardi, O. E.; Al-Belushi, M. I.; Al-Hajri, H. A.; Mahmoud, E. S.; Consolacion, E. C. Electrostatic Droplet Generation for Encapsulation of Somatic Tissue: Assessment of High-Voltage Power Supply. *Biotechnol. Prog.* **1997**, *13*, 497–502.

(48) Parmar, A. S.; Muschol, M. Hydration and Hydrodynamic Interactions of Lysozyme: Effects of Chaotropic Versus Kosmotropic Ions. *Biophys. J.* **2009**, *97*, 590–598.

(49) Seeber, S. J.; White, J. L.; Hem, S. L. Predicting the Adsorption of Proteins by Aluminium-Containing Adjuvants. *Vaccine* **1991**, *9*, 201–203.

(50) Tan, J.; Wang, Y.; Yip, X.; Glynn, F.; Shepherd, R. K.; Caruso, F. Nanoporous Peptide Particles for Encapsulating and Releasing Neurotrophic Factors in an Animal Model of Neurodegeneration. *Adv. Mater.* **2012**, *24*, 3362–3366.

(51) Radziejewski, C.; Robinson, R. C.; DiStefano, P. S.; Taylor, J. W. Dimeric Structure and Conformational Stability of Brain-Derived Neurotrophic Factor and Neurotrophin-3. *Biochemistry* **1992**, *31*, 4431–4436.

(52) Kuczewski, N.; Porcher, C.; Gaiarsa, J. L. Activity-Dependent Dendritic Secretion of Brain-Derived Neurotrophic Factor Modulates Synaptic Plasticity. *Eur. J. Neurosci.* **2010**, *32*, 1239–1244.

(53) Arriagada, F.; Correa, O.; Gunther, G.; Nonell, S.; Mura, F.; Olea-Azar, C.; Morales, J. Morin Flavonoid Adsorbed on Mesoporous Silica, a Novel Antioxidant Nanomaterial. *PLoS One* **2016**, *11*, e0164507.

(54) Mackie, A. R.; Macierzanka, A.; Aarak, K.; Rigby, N. M.; Parker, R.; Channell, G. A.; Harding, S. E.; Bajka, B. H. Sodium Alginate Decreases the Permeability of Intestinal Mucus. *Food Hydrocolloids* **2016**, *52*, 749–755.

(55) Schmidt, N.; Schulze, J.; Warwas, D. P.; Ehlert, N.; Lenarz, T.; Warnecke, A.; Behrens, P. Long-Term Delivery of Brain-Derived Neurotrophic Factor (BDNF) from Nanoporous Silica Nanoparticles Improves the Survival of Spiral Ganglion Neurons in Vitro. *PloS one* **2018**, *13*, e0194778.

(56) Yang, R.; Sabharwal, V.; Okonkwo, O. S.; Shlykova, N.; Tong, R.; Lin, L. Y.; Wang, W.; Guo, S.; Rosowski, J. J.; Pelton, S. I.; Kohane, D. S. Treatment of Otitis Media by Transtympanic Delivery of Antibiotics. *Sci. Transl. Med.* **2016**, *8*, 356ra120.

(57) Croissant, J. G.; Fatieiev, Y.; Khashab, N. M. Degradability and Clearance of Silicon, Organosilica, Silsesquioxane, Silica Mixed Oxide, and Mesoporous Silica Nanoparticles. *Adv. Mater.* **2017**, *29*, 1604634.

Table of Contents Graphic